J Mater Sci (2008) 43:7349–7353
DOI 10.1007/s10853-008-2813-9

High-pressure torsion for production of magnetoresistance in Cu–Co alloy

Kenichiro Suehiro · Shunichi Nishimura · Zenji Horita · Seiji Mitani · Koki Takanashi · Hiroyasu Fujimori

Received: 20 May 2008 / Accepted: 17 June 2008 / Published online: 13 July 2008

Abstract The process of high-pressure torsion (HPT) was applied to control the size and distribution of ferromagnetic Co particles in a Cu–Co alloy. Electron probe microanalysis, X-ray diffraction analysis, and transmission electron microscopy confirmed that the Co particles were significantly refined through fragmentation and dissolved with intense straining by HPT. Magnetoresistance appeared by ~2.5% at 77 K with an isotropic feature corresponding to giant magnetoresistance (GMR). It is demonstrated that HPT is a potential process for creating GMR in the Cu–Co alloy prepared by conventional ingot metallurgy.

Introduction

When ferromagnetic particles are finely dispersed in the matrix of non-magnetic materials, magnetoresistance (MR) appears with an isotropic feature in relative angles between magnetic field and electric current [1, 2], so that it is distinguished from anisotropic magnetorsistance (AMR) observed in conventional ferromagnets. The isotropic MR is called GMR if the MR ratio reaches more than a few tens of percents [1–8]. The Cu–Co system is known to be a good candidate for GMR as ferromagnetic Co particles with little solubility of Cu coexists in the Cu matrix according to the Cu–Co equilibrium phase diagram [9]. To achieve a fine dispersion of the ferromagnetic particles, several processes have been attempted such as thin film deposition following sputtering [1–3], meltspining from a molten alloy [4, 5], and mechanical milling of mixed powders [6–8]. For most cases, oversaturation was attained and therefore subsequent post-aging gave rise to a fine dispersion of Co particles in the Cu matrix. In this study, a process of high-pressure torsion (HPT) is used for a fine dispersion of Co particles. Because HPT is applicable to bulk metallic materials even with less ductile nature [10–13], this study demonstrates that HPT is a potential process for creating GMR in alloys prepared by conventional ingot metallurgy.

The HPT process is now widely known as a useful procedure for the microstructural refinement. Introducing intense shear strain in the sample through HPT, it is possible to refine not only the grain size but also the size and distribution including dissolution of the second-phase particles [14, 15]. As illustrated earlier [16], the facility for HPT generally consists of upper and lower anvils with shallow holes at the centers. A disk sample is placed on the hole and both anvils are rotated with respect to each other under application of high pressure. There are some other processes to introduce intense strain [17], such as Equal-Channel Angular Pressing (ECAP) [18] and Accumulative Roll Bonding (ARB) [19], but the HPT process has capability of producing finer microstructures than the other processes [20]. Nevertheless, most of the application of such intense straining processes have been made to the enhancement of mechanical properties such as the strength and ductility but there is limited application to functional

K. Suehiro · S. Nishimura · Z. Horita (✉)
Department of Materials Science and Engineering,
Faculty of Engineering, Kyushu University,
Fukuoka 819-0395, Japan
e-mail: horita@zaiko.kyushu-u.ac.jp

S. Mitani · K. Takanashi
Institute for Materials Research, Tohoku University,
Katahira 2-1-1, Sendai 980-8577, Japan

H. Fujimori
Research Institute for Electric and Magnetic Materials,
Sendai 982-0807, Japan

properties including magnetic properties [21–23].This study will then report the first attempt of the HPT process to refine microstructures of a Cu–Co alloy for the creation of GMR.

Experimental

An ingot with a composition of Cu–10 wt.%Co was prepared from high-purity Cu (99.99%) and high-purity Co (99.99%) using an arc-melting furnace in an argon atmosphere. The ingot with ~14 mm in diameter was swaged to a rod with 10.5 mm in diameter and homogenized at 1073 K for 24 h in an argon atmosphere. The rod was machined to a diameter of 10 mm and sliced to disks with thicknesses of 0.8 mm. HPT was conducted at room temperature with an applied pressure of 2.8 GPa. The lower anvil was rotated with respect to the upper at a rotation speed of 1 rpm for 5, 10 and 25 revolutions.

Microstrutcures were observed using electron probe microanalysis (EPMA) and transmission electron microscopy (TEM). For EPMA, after polishing the disk samples mechanically to a mirror-like surface, X-ray chemical mapping was conducted over areas of 100 × 100 μm^2 in outer regions located 0.5 mm from the disk edge where the shear straining was intense. A Shimazu EPMA-1600 was operated at 20 kV with a probe current of ~10 nA. For TEM, disks with 3 mm in diameter were punched out from the outer part of the HPT samples and ground mechanically to a thickness of 0.15 mm. They were further thinned in a solution of 15%HNO_3–70%CH_3OH–15%$C_3H_5(OH)_3$ under an applied voltage of 5–15 V at a temperature of 258 K using a twin-jet electropolishing apparatus. An H-8100 transmission electron microscope was operated under an accelerating voltage of 200 kV. X-ray diffraction (XRD) analysis was also performed at a condition of 40 kV and 36 mA using a Rigaku RINT-2100 with the Co-K_α line at a scanning speed of 0.2–0.4°min^{-1} and a step interval of 0.01°.

For MR measurement, a half ring having a width of 1.2 mm was cut from a disk sample as illustrated in Fig. 1 with an electric discharge machine. The electric resistance was measured with the half rings at a magnetic field of ±6 kOe using a four-point method at liquid nitrogen temperature (77 K) or at room temperature. The MR ratio was determined as

$$\text{MR ratio } (\%) = -100(R_{\max} - R_H)/R_{\max} \quad (1)$$

where R_H is the electric resistance at the application of magnetic field, H, and $R_{\max}$ is the maximum resistance in the measurement.

After the measurement of MR, a 1.2 mm × 1.4 mm square piece was cut from the middle part of the ring as illustrated in Fig. 1. This square piece was subjected to magnetization measurement using a Superconducting Quantum Interference Device (SQUID) magnetometer under a magnetic field of ±50 kOe. The magnetic field was applied in the directions parallel to X and Y as defined in Fig. 1.

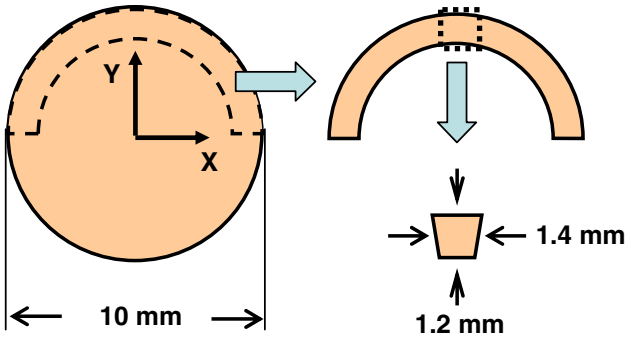

Fig. 1 Illustration of how to prepare samples for measurements of electrical resistance and magnetization including definition of X and Y directions

Results and discussion

Figure 2 shows X-ray chemical maps presenting Co distribution (a) after homogenization and after HPT for (b) $N = 5$, (c) $N = 10$, and (d) $N = 25$ revolutions. The gradations in color from blue through green to yellow and red indicate the increasing local enrichments of Co. It is apparent that the size of Co-rich regions decreases as the number of revolution increases. The initial size of Co particles after homogenization treatment but before HPT is ~20 μm. However, the particle size is decreased with an increase in the number of revolution and the Co particles become too small to be identified for the sample after 25 revolution. There may be a fraction that the Co particles are dissolved in the matrix.

Figure 3a shows XRD profiles after HPT for $N = 5$, 10, and 25 including the one after homogenization. All profiles are normalized by the peak height of the Cu(111) plane so that it is possible not only to check the presence of the Co phase but also its relative quantity in the matrix. Several Co peaks are present in the X-ray profile before HPT. They correspond to the (100), (002), and (101) planes of the Co phase having the hexagonal close packed (hcp) structure. However, close inspection reveals that there are also the Co peaks from the (111) and (200) planes in the face centered cubic (fcc) structure. The former fcc peak appears near the Cu(111) peak and the latter fcc peak near the Cu(200) peak. Although the distinction is difficult for the former peak because of the superposition with the Co(002) peak from the hcp structure, the presence of the latter is clearly

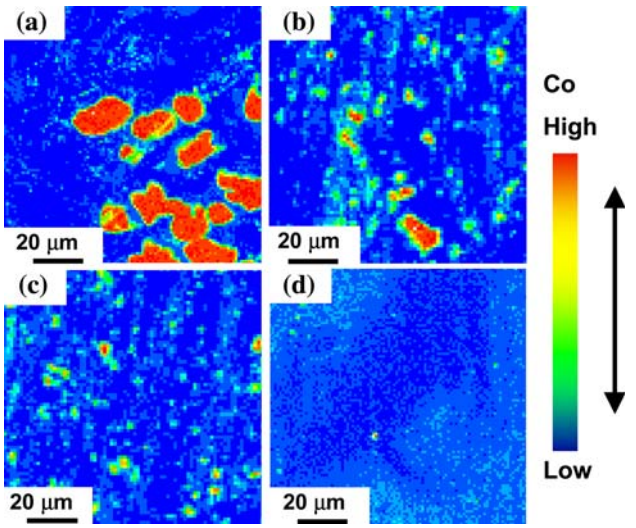

Fig. 2 EPMA X-ray Co mapping after (**a**) homogenization and after HPT revolutions of (**b**) $N = 5$, (**c**) $N = 10$, and (**d**) $N = 25$

demonstrated in the profiles enlarged near the Cu(200) peak as shown in Fig. 3b. It should be noted that the hcp Co is a stable phase but the fcc Co phase is an quasi-stable phase. The latter fcc Co phase has formed through the precipitation during homogenization as often observed in the past investigations [24, 25] and the fcc Co phase transforms into the hcp phase by deformation [26].

Now, checking the XRD profiles after HPT, it is important to emphasize that all Co peaks decrease with increasing number of the revolution from $N = 5$ to $N = 25$ and this is the case regardless of the crystal structures. This indicates that the Co-rich particles tend to disappear and be dissolved in the Cu matrix. The decrease in the Co peak height occurs more significantly for the (100) and (101) planes in the hcp structure and for the (200) planes from the fcc structure. However, as shown in Fig. 3c, the decrease in the Co peak from the (002) plane from hcp structure is gradual. This indicates that the (002) planes corresponding to the basal planes in the hcp structure are retained and it is thus suggested that the Co particles tend to exhibit a preferential orientation because of the straining by HPT made almost in the direction parallel to the disk plane.

A microstructure observed by TEM is shown in Fig. 4, where (a) is a bright files image and (b) a dark field image of the sample after $N = 25$. The observation was undertaken at a position 4 mm from the center of the disk. The dark-field image was recorded using a diffracted beam from the hexagonal Co(102) plane. The bright-field image shows that the grain size of the Cu matrix is $\sim$200 nm, while the dark-field image reveals that the Co particles are dispersed with the size of well less than 100 nm with an average interparticle spacing of $\sim$450 nm. It should be noted that the density of the particles should be higher because the dark-field image gives brighter contrast only

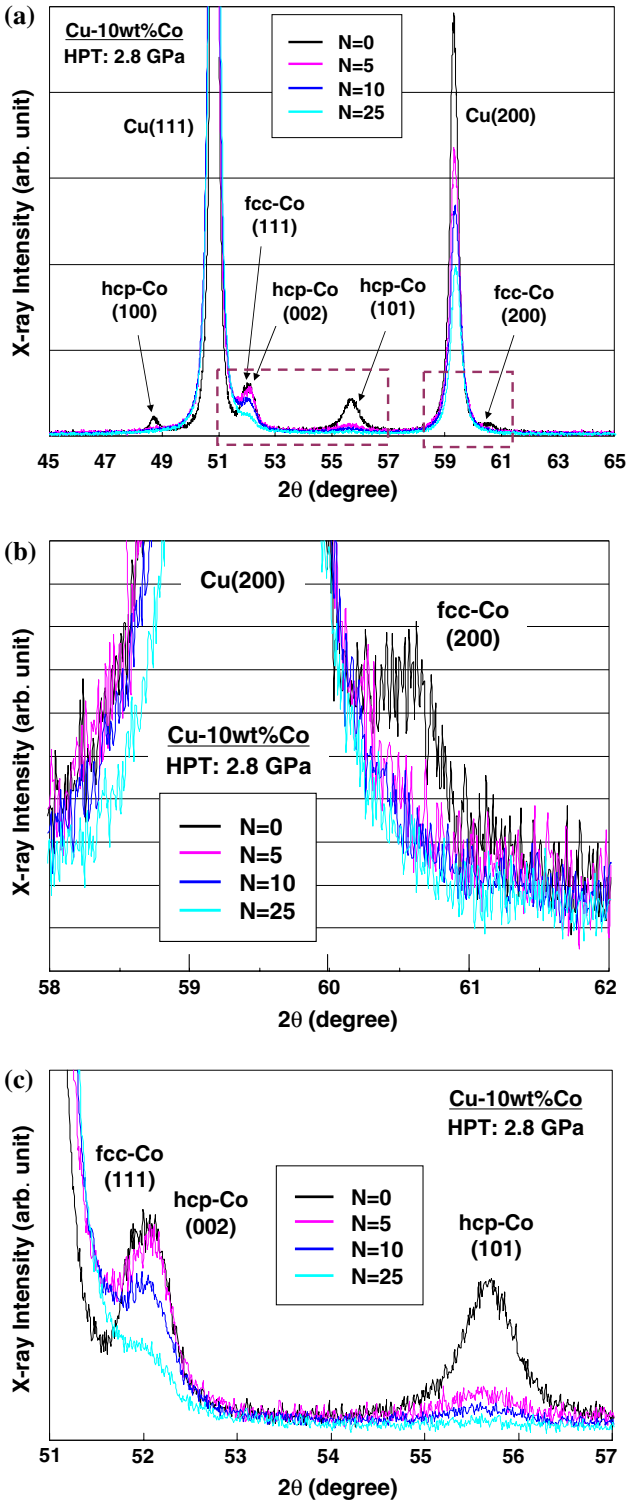

Fig. 3 (**a**) X-ray diffraction profiles after HPT revolutions of $N = 5$, $N = 10$, and $N = 25$ including after homogenization ($N = 0$). (**b**) Enlargement of X-ray diffraction profiles for $2\theta = 58$–$62°$. (**c**) Enlargement of X-ray diffraction profiles for $2\theta = 51$–$57°$

when the particles meet the diffraction condition but because the hcp Co particles from the other diffraction conditions including the fcc Co particles do not appear.

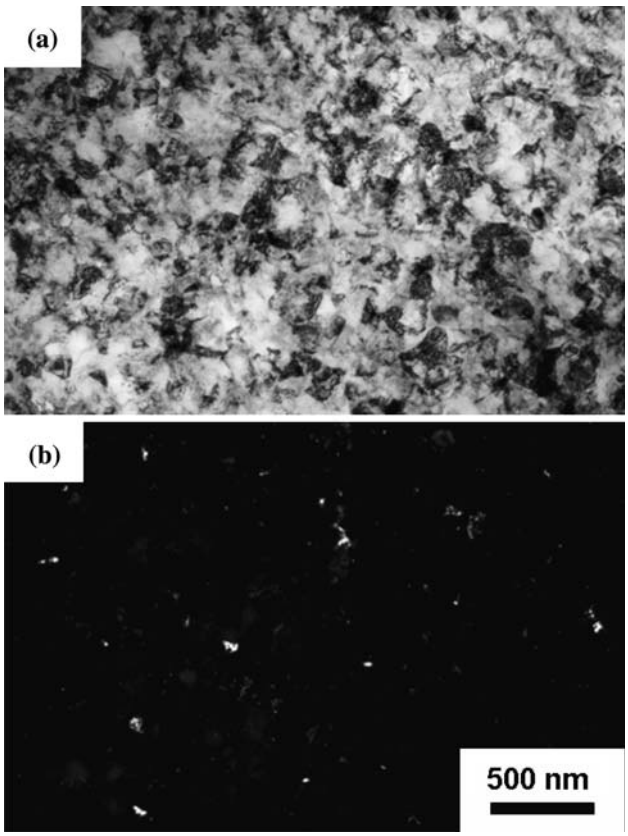

Fig. 4 Transmission electron micrograph after HPT revolutions of $N = 25$. (**a**) Bright-field image and (**b**) Dark-field image

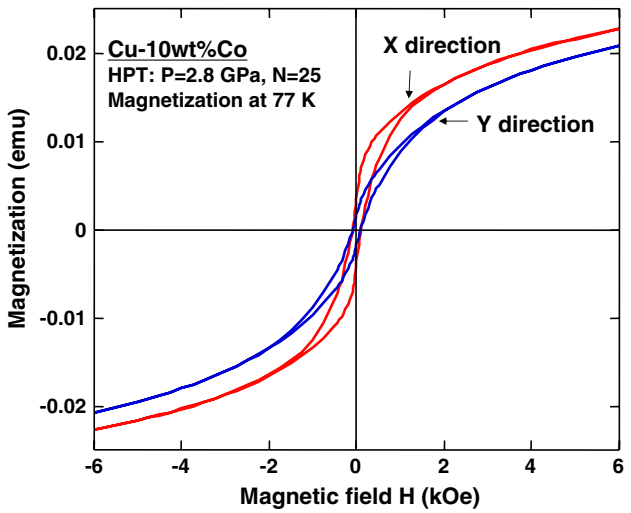

Fig. 5 Magnetization under application of magnetic field in X and Y directions defined in Fig. 2 for HPT sample after $N = 25$ revolutions

Figure 5 shows magnetic hysteresis loops obtained at 77 K under application of magnetic field in the directions parallel to the X and Y axes as defined in Fig. 1. Both loops look essentially similar to each other but the magnetization is slightly smaller when the magnetic field is applied in the X direction than in the Y direction. This must be due to the shear deformation along the circumference of the disk so that the Co particles can be elongated in the hoop direction.

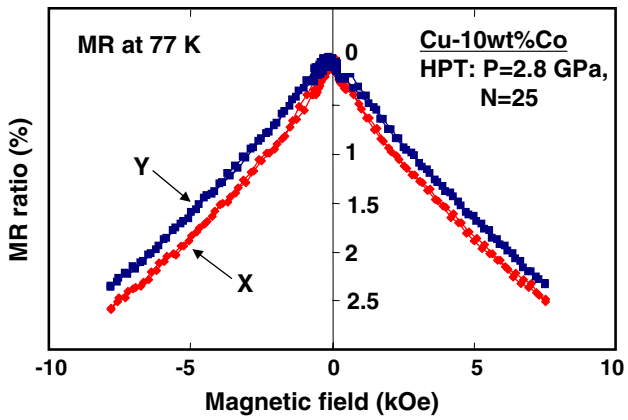

Fig. 6 Variation of MR ratio with magnetic field in X and Y directions defined in Fig. 2 for HPT sample after $N = 25$ revolutions

Figure 6 plots the MR ratio as a function of the magnetic field. The MR ratio reaches up to ~2.5% at 77 K. It is noted that the MR ratio at room temperature was ~0.25% and it was confirmed that no MR appeared before the HPT processing. There appears to be slight difference in the MR values obtained under applications of the magnetic field in the directions parallel to the X and Y directions as defined in Fig. 1. This difference cannot be explained as AMR in Co, which should lead to the larger resistance for the X direction (magnetic field // current), but is consistent with the anisotropy of the magnetization process as seen in the hysteresis loops shown in Fig. 5.

It was confirmed that such MR ratios were reproducible through repeated measurements. Although the MR ratios at the two temperatures are still insufficient for applications, it is emphasized that the MR ratios with a feature of GMR are obtained simply by the operation of HPT on samples prepared by conventional ingot metallurgy. It is suggested that aging the HPT samples may enhance the MR ratio because the dissolution of Co particles occurred and subsequently an oversaturation was attained by the HPT process. An optimization of aging condition is now undergoing.

Summary and conclusions

HPT was operated on a Cu alloy containing ferromagnetic Co particles. It was shown that the Co particles are fragmented to the nanometer size and even there is dissolution of the particles in the Cu matrix. It was confirmed that MR appears up to ~2.5% at 77 K with a feature of GMR. This study thus suggests that HPT is a potential process for attaining high values of GMR.

Acknowledgements This work was supported in part by a Grant-in-Aid for Scientific Research from the Ministry of Education, Culture, Sports, Science and Technology, Japan, in Priority Areas "Giant Straining Process for Advanced Materials Containing Ultra-High Density Lattice Defects" and in part by Kyushu University Interdisciplinary Programs in Education and Projects in Research Development (P&P).

References

1. Berkowitz AE, Mitchell JR, Carey MJ, Young AP, Zhang S, Spada FE et al (1992) Phys Rev Lett 68:3745. doi:10.1103/PhysRevLett.68.3745
2. Xiao JQ, Jiang JS, Chien CL (1992) Phys Rev Lett 68:3749. doi:10.1103/PhysRevLett.68.3749
3. Takanashi K, Park J, Sugawara T, Hono K, Goto A, Yasuda H et al (1996) Thin Solid Films 275:106. doi:10.1016/0040-6090(95)07064-8
4. Wang W, Zhu F, Weng J, Xiao J, Lai W (1998) Appl Phys Lett 72:1118. doi:10.1063/1.120942
5. Kim IJ, Takeda H, Echigoya J, Kataoka N, Fukamichi K, Shimada Y (1996) Mater Sci Eng A 217–218:363. doi:10.1016/S0921-5093(96)10347-6
6. Aizawa T, Zhou C (2000) Mater Sci Eng A 285:1. doi:10.1016/S0921-5093(00)00709-7
7. Larde R, Le Breton JM (2005) J Magn Magn Mater 290:1120. doi:10.1016/j.jmmm.2004.11.471
8. Rattanasakulthong W, Sirisathitkul C (2005) Physica B 369:160. doi:10.1016/j.physb.2005.08.010
9. Massalski TB, Murray JL, Bennett LH, Baker H, Kacprzak L (1987) Binary phase diagrams, vol 1. American Society of Metals, Metals Park, OH, p 758
10. Rentenberger C, Karnthaler HP (2005) Acta Mater 53:3031. doi:10.1016/j.actamat.2005.03.016
11. Waitz T, Kazykhanov V, Karnthaler HP (2004) Acta Mater 52:137. doi:10.1016/j.actamat.2003.08.036
12. Sabirov I, Pippan R (2005) Scr Mater 52:1293. doi:10.1016/j.scriptamat.2005.02.017
13. Kai M, Horita Z, Langdon TG (2008) Mater Sci Eng A 488:117
14. Senkov ON, Froes FH, Stolyarov VV, Valiev RZ, Liu J (1998) Nanostruct Mater 10:691. doi:10.1016/S0965-9773(98)00107-X
15. Sauvage X, Wetscher F, Pareige P (2005) Acta Mater 53:2127
16. Sakai G, Horita Z, Langdon TG (2005) Mater Sci Eng A 393:344. doi:10.1016/j.msea.2004.11.007
17. Valiev RZ, Estrin Y, Horita Z, Langdon TG, Zehetbauer MJ, Zhu YT (2006) JOM 58(4):33. doi:10.1007/s11837-006-0213-7
18. Segal VM, Reznikov VI, Drobyshevskiy AE, Kopylov VI (1981) Russ Metall 1:99
19. Saito Y, Utsunomiya H, Tsuji N, Sakai T (1999) Acta Mater 47:579. doi:10.1016/S1359-6454(98)00365-6
20. Dutkiewicz J, Kuśnierz J, Maziarz W, Lejkowska M, Garbacz H, Lewandowska M et al (2005) Phys Status Solidi 202:2309. doi:10.1002/pssa.200521235
21. Stolyarov VV, Gunderov DV, Popov AG, Puzanova TZ, Raab GI, Yavari AR et al (2002) J Magn Magn Mater 242–245:1399. doi:10.1016/S0304-8853(01)01244-6
22. Vorhauer A, Rumpf K, Granitzer P, Kleber S, Krenn H, Pippan R (2006) Mater Sci Forum 503–504:299
23. Suehiro K, Nishimura S, Horita Z (2008) Mater Trans 49:102. doi:10.2320/matertrans.ME200725
24. Servi IS, Turnbull D (1966) Acta Metall 14:161. doi:10.1016/0001-6160(66)90297-5
25. Fujii T, Tamura T, Kato M, Onaka S (2002) Microsc Microanal 8(Suppl. 2):1434CD
26. Suryanarayana C (2001) Prog Mater Sci 46:1. doi:10.1016/S0079-6425(99)00010-9